Optics Communications 366 (2016) 442–450

Contents lists available at ScienceDirect

Optics Communications

journal homepage: www.elsevier.com/locate/optcom

Spatial and spectral properties of entangled photons from spontaneous parametric down-conversion with a focused pump

Jong-Chan Lee, Yoon-Ho Kim

Department of Physics, Pohang University of Science and Technology (POSTECH), Pohang 790-784, Korea

ARTICLE INFO

Article history:
Received 30 October 2015
Received in revised form
18 December 2015
Accepted 19 December 2015
Available online 23 December 2015

Keywords:
Parametric down conversion
Entangled photon pair
Quantum state engineering

ABSTRACT

The spatial and spectral properties of entangled photons from spontaneous parametric down-conversion (SPDC) with a focused pump are investigated with theoretical analysis and numerical simulation. Here, the spatial and spectral properties of down-converted photons are fully calculated without using the transverse momentum conservation assumption. We have obtained the spatial and spectral properties of SPDC photons under focused pumping in various SPDC configurations, including type-I, type-II for both positive and negative uniaxial crystals. Our result not only helps to understand the effect of pump focusing in SPDC better but also can find use in application of SPDC in realizing quantum information protocols.

1. Introduction

For decades, spontaneous parametric down-conversion, or SPDC, has been an essential entangled photon source for quantum optics and photonic quantum information. One of the reasons why SPDC was used for many of the important scientific breakthroughs in the field of quantum optics is its versatility. SPDC is capable of producing entanglement in multiple degrees of freedom, including polarization [1], frequency [2], path [3], and orbital angular momentum [4]. Also, SPDC is known to be controllable to a great extent. Many degrees of freedom of SPDC photons can be prepared and controlled by carefully designing the experimental schematic and parameters, such as the choice of the non-linear crystals, inclination of the optic axis, spectral and spatial width of the pump laser. In particular, the properties of pump laser, both spectral and spatial, are important since they can rather be dynamically controlled unlike other static parameters. The properties of entangled photons from SPDC, including spectral and spatial properties [5–10], can be engineered by utilizing pump properties such as the pump spectrum [11–13] or the pump spatial profile [14–19]. Also, it is known that the coupling efficiency of SPDC photons to a single mode fiber can be optimized by properly adjusting the pump focusing condition [20–22]. The effect of pump focusing on the properties of SPDC photons, thus, recently has been an interesting issue for the application of SPDC in quantum optics and quantum information.

There have been several notable studies that dealt with the relation between the pump beam's spatial divergence, i.e. the pump focusing condition, and the properties of SPDC photons in some specific SPDC configurations. For instance, the effect of pump focusing on spectral properties of SPDC photons were studied for type-II SPDC in a beta-barium borate (BBO) crystal [14] and for type-I SPDC in a lithium iodate ($LiIO_3$) crystal [15]. The spatial profile of SPDC photons under the focused pumping is experimentally studied for type-II SPDC in a BBO crystal [17,18]. The near-field intensity profiles of type-I SPDC in focused pumping is studied by using classical wave equations [19]. In Ref. [19], however, the walk-off which may give the asymmetry in SPDC spatial profile is not included in the calculation. Although the previous studies may explain the changes in spectral and spatial properties due to the focused pump in some specific configurations, a more systematic approach that gives generalized description and prediction is still in need.

For the systematic description of SPDC with a focused pump, we calculated the quantum state of photon pairs of SPDC without using the transverse momentum conservation condition. The conservation of transverse momentum comes from the assumption that the interaction area on the crystal is very wide, typically many orders wider than the scale of the wavelength, and the pump intensity is nearly constant over this transverse region. Under this condition, as we show in the theory section in detail, the transverse integral can be written as

$$\int d^2r_\perp \exp[i(\vec{k}_{p\perp} - \vec{k}_{s\perp} - \vec{k}_{i\perp})\cdot\vec{r}_\perp] \approx \delta(\vec{k}_{p\perp} - \vec{k}_{s\perp} - \vec{k}_{i\perp}) \quad (1)$$

where $\vec{k}_{j\perp}$ are transverse momenta, $j = p, s, i$ means pump, signal and idler respectively. This is how the conservation of transverse momentum has originated. When we are considering focused

E-mail addresses: spiritljc@gmail.com (J.-C. Lee), yoonho72@gmail.com (Y.-H. Kim).

http://dx.doi.org/10.1016/j.optcom.2015.12.050
0030-4018/

pumping, the effective interaction area becomes relatively small, on the order of several tens of μm, and the pump intensity cannot be simply regarded as constant over the transverse region. In the focused pumping condition, in general, the conservation of transverse momentum assumption cannot be applied. To incorporate pump focusing conditions in SPDC, therefore, we have chosen to calculate the effect of pump focusing in SPDC without assuming the conservation of transverse momentum [23,24]. Note that it is also possible to decompose the state of the pump field into plane waves, where each plane wave satisfies the momentum conservation, for calculating the quantum state of SPDC [25–27].

In this paper, the spatial and spectral properties of entangled photons from SPDC with a focused pump are investigated in detail with theoretical analysis and numerical simulation. In the present calculation, transverse momentum conservation assumption is not used throughout the calculation so that it is possible to incorporate different pump focusing conditions. It can therefore gives a precise quantitative description on the spatial and spectral properties of SPDC with focused pump as well as the qualitative description. We have obtained the spatial and spectral properties of SPDC photons under focused pumping in various SPDC configurations, including type-I, type-II for both positive and negative uniaxial crystals. Our result not only helps understand the effect of pump focusing in SPDC better but also can be useful in applying SPDC to quantum information applications.

In Section 2, the properties of SPDC photons under focused pumping is theoretically calculated. The spatial profile and the spectral properties are numerically simulated and analyzed in detail in Section 3, based on the two-photon amplitude calculated in Section 2. By investigating the effect of pump focusing in various SPDC configurations, including type-I, type-II for both positive and negative uniaxial crystals, it became possible to better understand the causes responsible for the pump focusing effects. The paper is then summarized and concluded in Section 4.

2. Theory

The theoretical approach is based on a general SPDC scheme as shown in Fig. 1. A pump photon that comes into the non-linear crystal is annihilated and two SPDC photons are created. Then the generated SPDC photons are measured jointly at the detectors $D1$ and $D2$. The crystal, such as BBO, is aligned so that the optic axis lies in the plane made by the x axis and the pump propagation direction (z axis). The pump beam is focused through a focusing lens placed at a focal length ahead of the crystal. The crystal lies within the Rayleigh range so the beam width is assumed to be constant (w_0). To obtain different focusing conditions, one can change the focal length of the lens.

The relation between the wave vectors and the optic axis inside the crystal are shown in Fig. 2. The crystal is assumed to be uniaxial for simplicity. Here, z is set as the propagation direction of the pump beam, and the optic axis of the crystal is chosen to lie on $x-z$ plane making an angle Ψ with the z axis. A general wave vector inside the crystal can be fully specified by two angles: ψ and ϕ. Note that the photons polarized in $\hat{x}$ are called extraordinarily polarized photons, and those polarized in $\hat{y}$ are called ordinarily polarized photons. The refractive index for extraordinary photons depends both on the frequency and the propagating angle, $n_e(\omega_e, \theta)$, whereas that of ordinary photons depends only on the frequency, $n_o(\omega_o)$. Here, ω_e and ω_o are frequencies of extraordinary and ordinary photons, respectively.

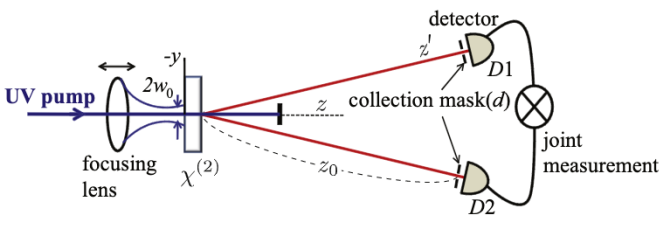

Fig. 1. A schematic of SPDC under focused pumping. The pump beam is focused by a lens and enters a nonlinear crystal. The down-converted photons travel to the detectors with collection masks and the coincidence between the two detectors is observed. w_0 is the beam width at the crystal, z_0 is the distance from the crystal to the detector, z is the pump propagation direction, z' is the direction of SPDC photons.

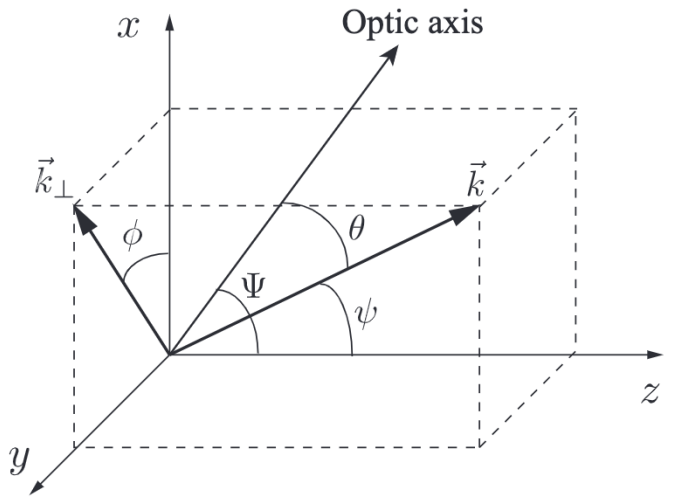

Fig. 2. The geometry of the crystal and the wave vector in SPDC process. The optic axis lies in the $x-z$ plane and θ is the angle between the propagation direction and optic axis.

In the interaction picture, the effective Hamiltonian of the SPDC process can be written as [28],

$$\mathcal{H} = \epsilon_0 \int d^3\vec{r}\, \chi^{(2)} E_p(\vec{r}, t) E_s^{(-)} E_i^{(-)} + h.c., \tag{2}$$

where the pump beam, $E_p(\vec{r}, t)$, is relatively intense so that it can be treated classically, and $E_s^{(-)}$, $E_i^{(-)}$ are quantized signal and idler photons inside the non-linear optical crystal, which is characterized by the 2nd order susceptibility $\chi^{(2)}$. The quantum state of SPDC can be calculated using the first order perturbation theory.

$$|\psi\rangle = -\frac{i}{\hbar}\int_{-\infty}^{\infty} dt\mathcal{H}|0\rangle, \tag{3}$$

where the vacuum contribution is dropped as it cannot be detected in the photon counting experiment.

What is often measured in the experiment is the average coincidence counting rate over a time interval T, which is known as [9],

$$R_c \propto \frac{1}{T}\int_0^T dT_1 \int_0^T dT_2 \left|\langle 0|E_1^{(+)}E_2^{(+)}|\psi\rangle\right|^2, \tag{4}$$

where $E_1^{(+)}$ and $E_2^{(+)}$ denote the quantized electromagnetic fields at the detectors (D1 and D2), t_1 and t_2 are the detection times at each detectors. The two-photon amplitude, or probability amplitude, is defined as,

$$\mathcal{A}_{12} \equiv \langle 0|E_1^{(+)}E_2^{(+)}|\psi\rangle. \tag{5}$$

The properties of generated photons can be studied by investigating the two-photon amplitude. In this section, we calculated the two-photon amplitude expression suitable for SPDC under the focused pumping condition.

We start by assuming that the input face of the crystal ($z=0$) is

parallel to the $x-y$ plane and that the pump beam is a monochromatic continuous wave. The pump field at the input face of the crystal is assumed to have a Gaussian profile,

$$E_p(\vec{r}_\perp, z=0, t=0) = \mathcal{E}_p \exp(-r_\perp^2/w_0^2), \tag{6}$$

where $\mathcal{E}_p$ is a constant, $r_\perp$ is the transverse position vector, and w_0 is the pump beam width. The pump beam inside the crystal can be written as [29]:

$$E_p(\vec{r}_\perp, z, t) = \int d^2k_{p\perp} \exp[-i\omega_p t] \times \exp[i(k_{pz}z + \vec{k}_{p\perp}\cdot\vec{r}_\perp)]\tilde{E}_p(\vec{k}_\perp) \tag{7}$$

where k_{pz} is the z component of pump wave-vector and $\vec{k}_{p\perp}$ is the transverse component of pump wave-vector. $\tilde{E}_p(\vec{k}_\perp)$ is the Fourier transform of the pump field at the front face of the crystal which is given as,

$$\tilde{E}_p(\vec{k}_\perp) = \mathcal{E}'_p \exp(-k_{p\perp}^2 w_0^2/4), \tag{8}$$

where $\mathcal{E}'_p$ is a constant. Here, it is non-trivial to simply integrate Eq. (7), since k_{pz} depends on transverse components of pump wave-vector as,

$$k_{pz} = \sqrt{\left(\frac{\omega_p}{c} n_e(\omega_p, \theta_p)\right)^2 - k_{px}^2 - k_{py}^2}, \tag{9}$$

where k_{pi} are the wave vector components in $i = x, y$ axis and θ_p is the angle between the optic axis and the pump direction as in Fig. 2.

Note that in the paraxial approximation k_{pz} can be approximated as [29]

$$k_{pz} \approx K_p\left[1 + \alpha_p\frac{k_{px}}{K_p} - \frac{1}{2}(1+\alpha_p\cot\Psi)\left|\frac{k_{p\perp}}{K_p}\right|^2 + \cdots\right], \tag{10}$$

where $K_p = \omega_p n_p(\omega_p, \Psi)/c$ is the magnitude of the pump wave vector when it is parallel to the z axis, and $\alpha_p = -\partial_\Psi \ln(n_p(\omega_p, \Psi))$ is the walk-off angle of the extraordinary pump beam. Note that for the ordinary pump beam, the walk-off angle vanishes as the refractivity is independent of the angle Ψ.

Under the paraxial approximation where $|k_{p\perp}/K_p| \ll 1$, the above expression can be approximated up to the first order as

$$k_{pz} \approx K_p + \alpha_p k_{px}. \tag{11}$$

Substituting Eq. (11) into Eq. (7), the pump field equation is calculated to be:

$$\begin{aligned} E_p(\vec{r}, t) &\approx \mathcal{E}'_p \exp[i(K_p z - \omega_p t)] \times \int dk_{px} \exp[i(\alpha_p z + x)k_{px}] \\ &\quad \exp(-k_{px}^2 w_0^2/4) \times \int dk_{py} \exp(ik_{py}y)\exp(-k_{py}^2 w_0^2/4) \\ &= \mathcal{E}'_p \exp[i(K_p z - \omega_p t)] \exp\left[-\frac{(\alpha_p z + x)^2 + y^2}{w_0^2}\right]. \end{aligned} \tag{12}$$

Above equation indicates that the center of the beam is shifted from $x=0$ to $x = -\alpha_p z$ as the beam propagates through the crystal in the z direction: pump walk-off.

In general, the propagation direction of SPDC photons is different from the pump direction. The reference frames defined for the pump and the SPDC photons are shown in Fig. 3. Here, the SPDC photons are assumed to be propagating in z' direction, which is fully defined by two angles (ϕ_j, ψ_j). The axis x' and y' are chosen so that the optic axis lies on the $x'-z'$ plane. The refractive index of an extraordinary photon depends on Ψ_j, where the subscript j refer either the signal or the idler photons.

Now, the negative frequency component of the quantized SPDC field can be represented in the primed reference frame:

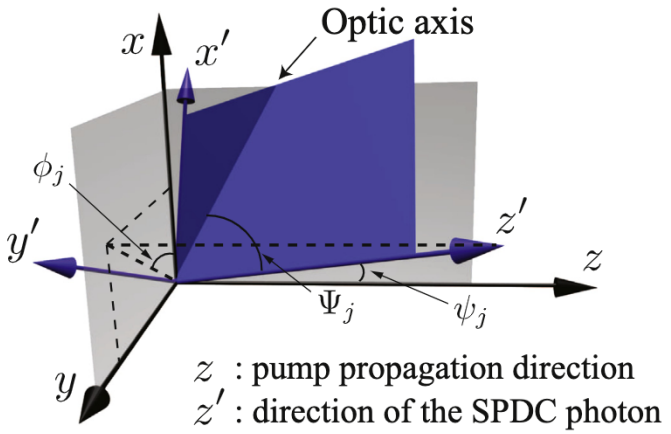

Fig. 3. The reference frames of the pump beam (unprimed frames) and that of the SPDC photons (primed frames). x' and y' are selected such that the crystal's optic axis lies in $x'-z'$ plane. The subscript j represents signal or idler photons.

$$E_j^{(-)}(\vec{r}, t) = \int d^3k'_j\, \mathcal{E}_j a^\dagger_{k'j} \exp[-i(\vec{k}'_j\cdot\vec{r}' - \omega_j t)] \tag{13}$$

where $\mathcal{E}_j$ is a constant, $a^\dagger_{k'j}$ is a creation operator of the photon with wave vector k'_j. Therefore, by combining Eq. (12), Eq. (13) with Eq. (2), the Hamiltonian can be re-written as,

$$\begin{aligned} H \propto \int d^3\vec{r} \int d^3k_s \int d^3k_i \exp[i(K_p z - \omega_p t)] \times \\ \exp\left[-\frac{(\alpha_p z + x)^2 + y^2}{w_0^2}\right] a^\dagger_{k's} a^\dagger_{k'i} \exp[-i(\vec{k}'_s\cdot\vec{r}' - \omega_s t)] \\ \times \exp[-i(\vec{k}'_i\cdot\vec{r}' - \omega_i t)] + h.c., \end{aligned} \tag{14}$$

and by using Eq. (3), the long interaction time assumption, the quantum state of SPDC is calculated to be

$$\begin{aligned} |\psi\rangle \propto \int d^3\vec{r} \int d^3k_s \int d^3k_i \\ a^\dagger_{k's} a^\dagger_{k'i} \delta(\omega_p - \omega_s - \omega_i) \times \exp[i(K_p z - \vec{k}'_s\cdot\vec{r}' - \vec{k}'_i\cdot\vec{r}')] \\ \exp\left[-\frac{(\alpha_p z + x)^2 + y^2}{w_0^2}\right]|0\rangle, \end{aligned} \tag{15}$$

where the $\delta(\omega_p - \omega_s - \omega_i)$ term comes from the integral over time.

Let us now calculate the two-photon amplitude $\mathcal{A}_{12} = \langle 0|E_1^{(+)}E_2^{(+)}|\psi\rangle$. In the two-photon amplitude calculation, the quantized field at the detectors $E_1^{(+)}$ and $E_1^{(+)}$ should be considered. Note that, as shown in Fig. 1, the SPDC photons travel nearly collinearly to the detectors D_1 and D_2, which are typically located at the far-zones from the source. We assume a pinhole or a collection mask before each detector, which reflects the finite detector size. Considering the collection mask to be infinitesimal, the electric field operator of the SPDC photon at the detector $D1$ can be written as

$$E_1^{(+)}(\vec{r}, t) = \int d^3k'_m\, a_{k'm} \exp[i(\vec{k}'_m\cdot\vec{r}' - \omega_m t_1)]\delta(\vec{k}'_{m\perp}), \tag{16}$$

where the subscript m refer to signal or idler, t_1 is the time at which the photon arrive the detector $D1$ and $a_{k'm}$ is the annihilation operator of the photon with momentum $\vec{k}'_m$ at $D1$. In this paraxial collection setting, the wave vector of SPDC photons in z' direction can be written as,

$$k'_{mz} \approx K'_m, \tag{17}$$

where K'_m is the magnitude of the wave vector when the photon propagates exactly in the z' direction. Consequently, the field that arrives at detector $D1$, $E_1^{(+)}$, can be approximated to be,

$$E_1^{(+)}(\vec{r}, t) \propto \int d\omega_m\, a_{k'm} \exp[i(K'_m z_1 - \omega_m t_1)] = \int d\omega_m\, a_{k'm} \exp[-i\omega_m T_1], \tag{18}$$

where z_1 is the distance from the crystal to the detector 1 and $T_1 = t_1 - z_1/c$. The field at the detector $D2$, $E_2^{(+)}$, can also be calculated in the same manner.

The two-photon amplitude, $\mathcal{A}_{12} = \langle 0|E_1^{(+)}E_2^{(+)}|\psi\rangle$, can now be estimated by using Eqs. (15) and (18). There is a commutation relation between the creation and annihilation operators, $[a_{km}, a_{kj}^{\dagger}] = \delta(\vec{k}_m - \vec{k}_j)$, which can be used in the integration. This greatly reduces the complexity in calculating the two-photon amplitude, which is given as

$$\mathcal{A}_{12} \propto \int d\omega_s \int d\omega_i \int d^3\vec{r}\; \delta(\omega_p - \omega_s - \omega_i) \times \exp[i(K_p z - K'_s z'_s - K'_i z'_i)] \exp\left[-\frac{(\alpha_p z + x)^2 + y^2}{w_0^2}\right] \times \exp[-i(\omega_s T_1 + \omega_i T_2)], \tag{19}$$

where $z'_{s,i}$ are the propagation directions of signal and idler photons. By using the geometric identity,

$$K'_j z'_j = K'_j \sin\psi_j \cos\phi_j\, x + K'_j \sin\psi_j \sin\phi_j\, y + K'_j \cos\psi_j\, z, \tag{20}$$

where the angles ψ_j, ϕ_j, Ψ_j are defined in Fig. 3. The probability amplitude $\mathcal{A}_{12}$ then becomes,

$$\mathcal{A}_{12} \propto \int d\omega_s \int d\omega_i \int dx dy dz\; \delta(\omega_p - \omega_s - \omega_i) \times \exp(-i[\Delta_x x + \Delta_y y - \Delta_z^o z]) \exp\left[-\frac{(\alpha_p z + x)^2 + y^2}{w_0^2}\right]. \tag{21}$$

where the unimportant phase component, $\exp[-i(\omega_s T_1 + \omega_i T_2)]$, is neglected and we define the phase mismatches Δ_x, Δ_y, Δ_z^o, Δ_z as,

$$\begin{aligned}
\Delta_x &\equiv K'_s(\omega_s, \Psi_s)\sin\psi_s \cos\phi_s + K'_i(\omega_i, \Psi_i)\sin\psi_i \cos\phi_i \\
\Delta_y &\equiv K'_s(\omega_s, \Psi_s)\sin\psi_s \sin\phi_s + K'_i(\omega_i, \Psi_i)\sin\psi_i \sin\phi_i \\
\Delta_z^o &\equiv K_p(\omega_p, \Psi) - K'_s(\omega_s, \Psi_s)\cos\psi_s - K'_i(\omega_i, \Psi_i)\cos\psi_i \\
\Delta_z &\equiv \Delta_z^o + \alpha_p \Delta_x.
\end{aligned} \tag{22}$$

The spatial integration in Eq. (21) can be separated into three directions, x, y, and z. As the cross-sectional area of the crystal is big enough to cover the interaction area, which is defined by the pump beam width w_0, we can simply take the transverse integral range as infinity. Here we used the change of basis method by defining $\tilde{x} = x + \alpha_p z$ instead of x. Since α_{pz} is much smaller than the cross-section of the crystal, the integration range of $\tilde{x}$ may be regarded as infinity as well. This results in,

$$\begin{aligned}
&\int_{-\infty}^{\infty} dx\; \exp\left[-\frac{(\alpha_p z + x)^2}{w_0^2}\right] \exp[-i\Delta_x x] \\
&= \int_{-\infty}^{\infty} d(\alpha_p z + x) \exp\left[-\frac{(\alpha_p z + x)^2}{w_0^2}\right] \exp[-i\Delta_x\{(\alpha_p z + x) - \alpha_p z\}] \\
&= \int_{-\infty}^{\infty} d\tilde{x}\; \exp\left[-\frac{\tilde{x}^2}{w_0^2}\right] \exp[-i\Delta_x\{\tilde{x} - \alpha_p z\}] \\
&= \exp[i\Delta_x \alpha_p z] \exp\left[-\frac{w_0^2 \Delta_x^2}{4}\right].
\end{aligned} \tag{23}$$

Likewise the y component of integration becomes,

$$\int_{-\infty}^{\infty} dy \exp\left[-\frac{y^2}{w_0^2}\right] \exp[-i\Delta_y y] = \exp\left[-\frac{w_0^2 \Delta_y^2}{4}\right]. \tag{24}$$

In the z direction, the crystal of length L lies between $z=0$ and $z=L$. Considering the result in Eq. (23) together with Eq. (21), the integration in the z direction becomes

$$\int_0^L dz \exp[i(\Delta_z^o + \alpha_p \Delta_x)] = L\,\mathrm{sinc}(L\Delta_z/2)\exp(iL\Delta_z/2). \tag{25}$$

Now we can calculate the two-photon amplitude expression by inserting Eqs. (23)–(25) into Eq. (21). The two-photon amplitude is calculated to be

$$|\mathcal{A}_{12}| \propto \int d\omega_s \int d\omega_i\, \delta(\omega_p - \omega_s - \omega_i) \times \exp[-w_0^2(\Delta_x^2 + \Delta_y^2)/4]\, \mathrm{sinc}(L\Delta_z/2). \tag{26}$$

There are six independent variables in Eq. (26): ψ_s, ϕ_s, ψ_i, ϕ_i, ω_s, w_0. Among them, first four variables, ψ_s, ϕ_s, ψ_i, ϕ_i, are determined by the location of the detectors in the angular plane. It will be discussed in detail in the following section how to uniquely determine the variables with detector positions. For the cw pump beam, ω_s defines the frequency of the signal photon as well as that of the idler photon, due to the strong frequency anti-correlation, $\delta(\omega_p - \omega_s - \omega_i)$. The last variable w_0 is pump beam width, which determines the pump focusing condition; hence, it is the most relevant variable in our calculation. Note that, throughout the calculation, the conservation of transverse momentum conservation assumption, in other words, $\delta(\vec{k}_{p\perp} - \vec{k}_{s\perp} - \vec{k}_{i\perp})$, has never been used.

3. Results and discussion

We now numerically simulate our result by using the two-photon amplitude calculated in Eq. (26). The coincidence count is simply the absolute square of two-photon amplitude $|\mathcal{A}_{12}|^2$ integrated over detection time (Eq. (4)), which can typically be assumed as infinity [9]. We used two different crystals with different characters for simulation: BBO and Urea. BBO is a negative uni-axial crystal and Urea is a positive uni-axial crystal, respectively. The numerical simulations performed in this section are based on the Sellmeier equations of BBO and Urea, which can be found in Ref. [30,31]. In the simulation, the length of the crystal is assumed to be 3 mm. Also, it is assumed that the pump beam is a monochromatic continuous wave at 405 nm.

Let us describe how the spatial profile of SPDC photons are obtained by the numerical simulation method. To see the spatial profile in the angular plane, we have to define the angles in the angular plane, θ_x and θ_y, and relate the angles with the angles in the two-photon amplitude, ψ_j and ϕ_j, where the subscript j refers to signal s and idler i. See, Fig. 3. The angles θ_x, θ_y are uniquely defined from the geometry as,

$$\begin{aligned}
\tan\phi_j &= \frac{\tan\theta_y}{\tan\theta_x} \\
\tan\psi_j^{out} &= \sqrt{\tan^2\theta_x + \tan^2\theta_y}
\end{aligned} \tag{27}$$

where $\psi_j^{out} = \sin^{-1}(n_j(\omega_j, \Psi_j)\sin\psi_j)$ denotes the angle of the detector from z axis, seen outside the crystal. Then one can calculate the angles Ψ_j and ψ_j from θ_x and θ_y by employing the geometrical identity,

$$\cos\Psi_j = \cos\Psi\cos\psi_j + \sin\Psi + \sin\psi_j\cos\phi_j. \tag{28}$$

Hence, when two detector positions are determined in the angular plane, we can estimate the corresponding four angle values inside the crystal (ψ_s, ϕ_s, ψ_i, ϕ_i) which are required for calculating two-photon amplitude. Now, when the focusing condition is determined (w_0) and the signal, idler wavelengths are set, the detection probability of SPDC can be obtained as $|\mathcal{A}_{12}|^2$. Note, in our discussion, we assumed that the optic axis is aligned for the frequency degenerate SPDC case, i.e. $\lambda_s = \lambda_i = \lambda_0 = 810$ nm. Also, for

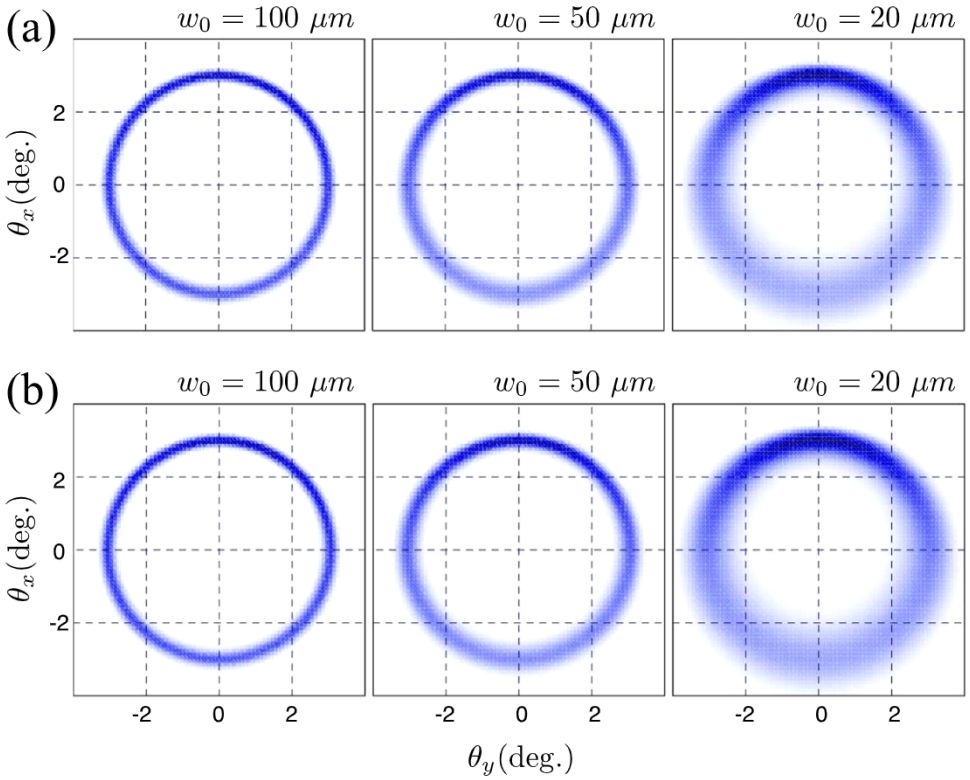

Fig. 4. Spatial profiles of non-collinear ($\theta_y = 3°$) type-I SPDC under different pump focusing conditions. The SPDC is assumed to take place in (a) negative uni-axial crystal (BBO), (b) positive uni-axial crystal (Urea). It is clearly seen that in both cases, the spatial pattern of SPDC becomes broader and asymmetric as the pump gets more tightly focused. The broadening effect is asymmetric in the θ_x direction, whereas it is symmetric in the θ_y direction. Although the broadening direction looks identical in both cases, by carefully investigating the two-photon amplitude, we know that the actual cause for each case is different. In negative uni-axial crystal (a), the pump walk-off is the main reason for the asymmetry. However, in positive uni-axial crystal, SPDC photon's walk-off is the main reason for asymmetry.

simplicity, we assumed that a narrow bandpass filter, $\delta(\lambda_s - \lambda_0) = \delta(\lambda_i - \lambda_0)$, is located in front of the detectors. Finally, we numerically integrate the two-photon amplitude as given in Eq. (26) to calculate the detection probability of SPDC.

Let us now discuss the numerical simulation results. Fig. 4 (a) and (b) shows the spatial profile of type-I SPDC under different pump focusing conditions, $w_0 = 100\,\mu$m, $50\,\mu$m, $20\,\mu$m, in a negative uni-axial (BBO) and a positive uni-axial crystal (Urea), respectively. Note, in the simulation, the optic axis is set to lie in $+\theta_x$ direction. It is clearly observable that the spatial pattern of SPDC becomes broader and asymmetric as the pump gets more tightly focused. Note that the broadening effect is asymmetric in the θ_x direction, whereas it is symmetric in the θ_y direction. Although the broadening seems to be similar in both crystals, the reasons for broadening are different from each other. To understand the asymmetry, we now consider the two crystal choices separately.

Let us first look at the negative uni-axial crystal, BBO, see Fig. 4 (a). Type-I SPDC in BBO is converting one extraordinarily polarized pump photon into two ordinarily polarized photons ($e \to o + o$). The pump beam has the walk-off in the $-\theta_x$ direction. Recall that K_s' and K_i' in Eq. (22) do not have angular dependence as they are ordinary photons. To probe where the asymmetry in case of negative uni-axial crystal originates, we intentionally changed the sign of θ_x. When θ_x changes to $-\theta_x$, ϕ_j changes into $\pi - \phi_j$ whereas ψ_j do not change. The corresponding phase mismatches will change as,

$$\begin{aligned}\Delta_x &\to -\Delta_x\\ \Delta_y &\to \Delta_y\\ \Delta_z &\to \Delta_z^o - \alpha_p\Delta_x.\end{aligned} \tag{29}$$

so that the sinc function in two-photon amplitude, Eq. (26), changes to be

$$\mathrm{sinc}(L\Delta_z/2) \to \mathrm{sinc}[L(\Delta_z^o - \alpha_p\Delta_x)/2]. \tag{30}$$

Since the two-photon amplitude changes when we change the sign of θ_x, there is no symmetry along θ_x so the spatial profile should be asymmetric as in Fig. 4(a). This asymmetric effect is originated from the pump walk-off α_p. Note that $-\theta_x$ direction is more broadened than $+\theta_x$ direction. In negative uni-axial BBO crystal, hence, the walk-off direction is the same as the direction that the SPDC ring is more broadened.

Second, let us take a look at the positive uni-axial case, Fig. 4 (b). In a positive uni-axial crystal, Urea, one ordinary pump photon is down-converted into two extraordinary SPDC photons ($o \to e + e$). The pump beam do not have the walk-off, $\alpha_p = 0$, since it is ordinary while the generated photons do have angular dependence on the refractive index. The following phase mismatches can be written as,

$$\begin{aligned}\Delta_x &\equiv K_s'(\omega_s, \Psi_s)\sin\psi_s\cos\phi_s + K_i'(\omega_i, \Psi_i)\sin\psi_i\cos\phi_i\\ \Delta_y &\equiv K_s'(\omega_s, \Psi_s)\sin\psi_s\sin\phi_s + K_i'(\omega_i, \Psi_i)\sin\psi_i\sin\phi_i\\ \Delta_z &\equiv K_p(\omega_p) - K_s'(\omega_s, \Psi_s)\cos\psi_s - K_i'(\omega_i, \Psi_i)\cos\psi_i.\end{aligned} \tag{31}$$

Let us first check the symmetry of θ_y direction by substituting $-\theta_y$ for θ_y. Since the refractive indices of signal and idler photons have angle dependence, i.e. $K_j'(\omega_j, \Psi_j) = \omega_j n_j(\omega_j, \Psi_j)/c$, we also have to consider the change of angle Ψ_j where $j = s, i$. According to Eq. (27) and (28), the angle Ψ_j do not change under the sign change of θ_y. The change of the phase mismatches are given as,

$$\Delta_x \to \Delta_x$$
$$\Delta_y \to -\Delta_y$$
$$\Delta_z \to \Delta_z, \tag{32}$$

resulting in the unchanged two-photon amplitude. Therefore, the spatial profile of type-I SPDC in a positive uni-axial crystal is symmetric in θ_y direction just like that in a negative uni-axial crystal.

Then, let us substitute $-\theta_x$ for θ_x. According to Eqs. (27) and (28), the angle responsible for the refractive index of SPDC photons, Ψ_j, changes with the relation,

$$\Psi_j \to \cos^{-1}\left(\cos\Psi\cos\psi_j + \sin\Psi - \sin\psi_j\cos\phi_j\right). \tag{33}$$

The phase mismatches, $\Delta_{x,y,z}$, becomes different for the change of sign in θ_x, hence the two-photon amplitude is not symmetric in θ_x. The asymmetry in two-photon amplitude implies that the spatial profile along θ_x would be asymmetric. Just to give more intuition, let us expand K_j' as a function of Ψ.

$$K_j'(\omega_j, \Psi_j) \approx K_j\left[1 + \alpha_j\frac{k_{jx}}{K_j} - \frac{1}{2}(1 + \alpha_j\cot\Psi)\left|\frac{k_{j\perp}}{K_j}\right|^2 + \cdots\right], \tag{34}$$

where $K_j = \omega_j n_j(\omega_j, \Psi)/c$ is the magnitude of signal or idler wave vector if it is parallel to the z axis and $\alpha_j = -\partial_\Psi \ln(n_j(\omega_j, \Psi))$ is the walk-off of the SPDC photons. If we only consider the first order in $k_{j\perp}/K_j$,

$$K_j'(\omega_j, \Psi_j) \approx K_j + \alpha_j k_{jx}. \tag{35}$$

When the sign changes in θ_x, then the walk-off component changes sign as,

$$K_j'(\omega_j, \Psi_j) \approx K_j - \alpha_j k_{jx}, \tag{36}$$

giving the asymmetric spatial profile in θ_x. This gives a simple analogue to the pump walk-off, which provides an intuitive way of understanding asymmetric broadening of spatial profiles.

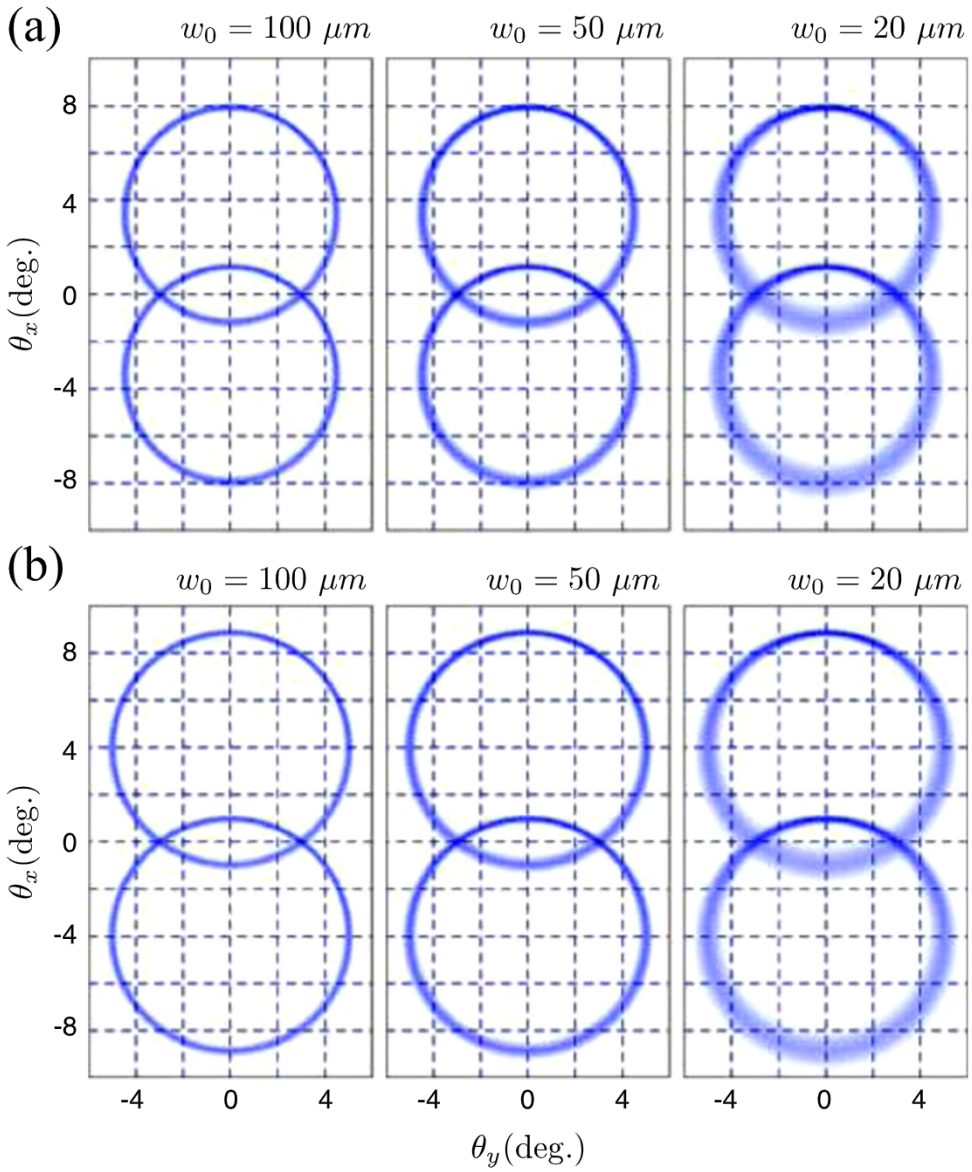

Fig. 5. Spatial profiles of non-collinear (3 °) type-II SPDC under different pump focusing conditions with different crystals: (a) BBO, (b) Urea. Each grid is scaled to 2 degrees. Here, it is shown that the pump focusing makes SPDC photons' spatial profile broad asymmetrically. Here again, as in type-I case, the broadening effect looks identical in (a) and (b). However, the situation is not as simple as in type-I. For type-II SPDC in negative uni-axial crystal (a), the pump walk-off and the SPDC photon's walk-off are both present. In this case, the pump walk-off prevails, so the asymmetric direction is pump beam's walk-off direction. For type-II SPDC in positive uni-axial crystal (b), only SPDC photons have walk-off, hence it is the only cause of the asymmetry.

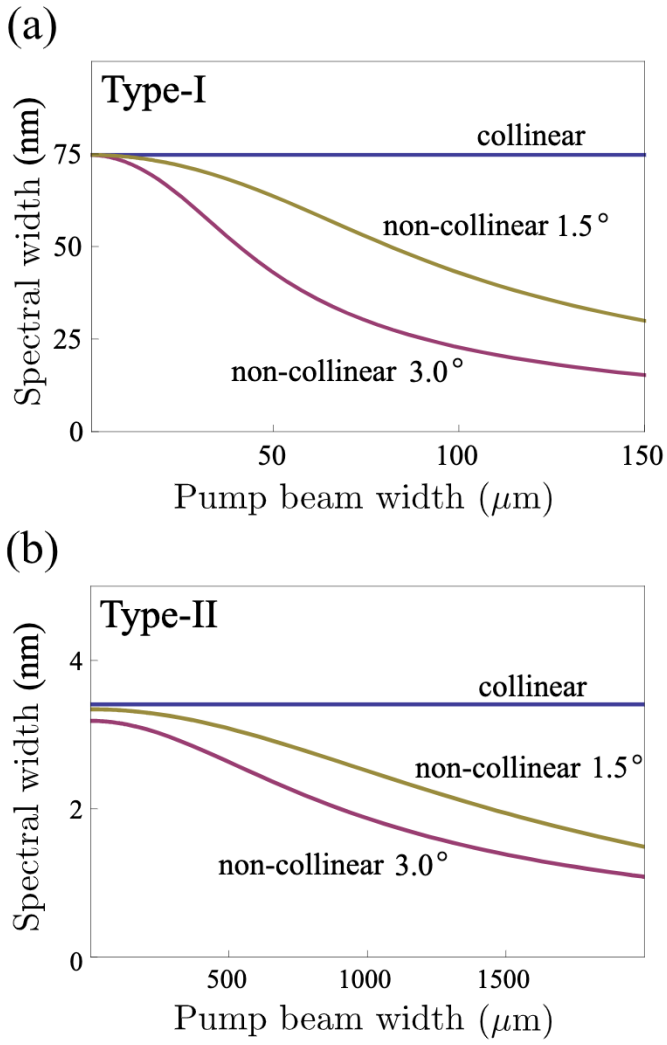

Fig. 6. The spectral width (FWHM) of down-converted photons as a function of pump beam width. (a) The spectral width of the collinear and non-collinear (1.5 °, 3 °) Type-I SPDC. (b) The spectral width of the collinear and non-collinear (1.5 °, 3 °) Type-II SPDC.

However, note that the actual numerical simulation must not approximate K_j' as in Eq. (35), but rather all orders of Eq. (34) should be considered. In non-collinear settings, the emission angles of down-converted photons, i.e. $k_{j\perp}/K_j$, can routinely be more than a few degrees. Hence, we cannot simply ignore $k_{j\perp}$ by assuming that $k_{j\perp}/K_j \ll 1$. Also note that the walk-off direction in a positive uni-axial Urea crystal is $+\theta_x$, whereas the direction where the spatial profile is more broadened is $-\theta_x$. In positive uni-axial Urea crystal, therefore, the walk-off direction is the opposite of the direction that the SPDC ring is more broadened.

In Fig. 4(b), the change of spatial profile of type-I SPDC in a positive uni-axial crystal (Urea) is shown. Similar to the negative uni-axial case, Fig. 4(a), the broadening effect is symmetric in θ_y direction, but asymmetry appears in θ_x: the $-\theta_x$ direction is more broadened than $+\theta_x$ direction. In the positive uni-axial crystal, Urea, the walk-off of SPDC photons are responsible for asymmetric broadening not the pump walk-off. It is noticeable that not only the pump walk-off, but also the walk-off of SPDC photons are responsible for the asymmetric changes in spatial profile due to pump focusing.

Let us now study the case for type-II SPDC. In Fig. 5, spatial profile of type-II non-collinear SPDC under focused pumping is demonstrated with a negative uni-axial (BBO) and with a positive uni-axial crystal (Urea). The spatial profiles of SPDC are more broadened as the pump becomes more focused, from $w_0 = 100\,\mu$m to $w_0 = 20\,\mu$m. Here, asymmetry in spatial mode broadening is clearly observable. Fig. 5(a) shows the changes in spatial profile of type-II SPDC in a negative uni-axial crystal, BBO. The pump photon is extraordinary and the generated photons are an ordinary and an extraordinary photon ($e \rightarrow e + o$). In this condition, the phase mismatches are,

$$\begin{aligned}
\Delta_x &\equiv K_s'(\omega_s, \Psi_s)\sin\psi_s \cos\phi_s + K_i'(\omega_i)\sin\psi_i \cos\phi_i \\
\Delta_y &\equiv K_s'(\omega_s, \Psi_s)\sin\psi_s \sin\phi_s + K_i'(\omega_i)\sin\psi_i \sin\phi_i \\
\Delta_z^o &\equiv K_p(\omega_p, \Psi) - K_s'(\omega_s)\cos\psi_s - K_i'(\omega_i)\cos\psi_i \\
\Delta_z &\equiv \Delta_z^o + \alpha_p \Delta_x. \qquad (37)
\end{aligned}$$

One can easily figure out that the two-photon amplitude is symmetric in θ_y direction, but the asymmetry in θ_x may not be clearly understood since there are two components that walk off: pump and one SPDC photon. From the numerical simulation, it turned out that the pump walk-off prevails, so the spatial profile is more broadened in $-\theta_x$ direction, as in Fig. 4(a) case.

Then, let us take a look at the positive uni-axial crystal case in Fig. 5(b). In type-II SPDC in a positive uni-axial crystal, Urea, an ordinary pump photon is down-converted into an ordinary and an extraordinary photon ($o \rightarrow e + o$). Note that the pump beam do not have walk-off, and the signal photon is assumed to be extraordinary while the idler is assumed to be ordinary. The phase mismatches will be,

$$\begin{aligned}
\Delta_x &\equiv K_s'(\omega_s, \Psi_s)\sin\psi_s \cos\phi_s + K_i'(\omega_i)\sin\psi_i \cos\phi_i \\
\Delta_y &\equiv K_s'(\omega_s, \Psi_s)\sin\psi_s \sin\phi_s + K_i'(\omega_i)\sin\psi_i \sin\phi_i \\
\Delta_z &\equiv K_p(\omega_p) - K_s'(\omega_s, \Psi_s)\cos\psi_s - K_i'(\omega_i)\cos\psi_i. \qquad (38)
\end{aligned}$$

The symmetry of the spatial profile in θ_y direction can be easily seen. Due to the walk-off of the signal photon, the spatial profile becomes asymmetric in θ_x as shown in Fig. 5(b); $-\theta_x$ direction is more broadened than $+\theta_x$. Note that although only one of the photons is the extraordinary photon which walks off, both of the photon rings are broadened in a similar way.

So far, we have observed that the spatial profiles of SPDC photons under focused pumping are asymmetric and broadened than the original spatial profile in both positive and negative uni-axial crystals. This asymmetric broadening effect can affect the quality of photon pairs when using it in quantum interferometry or quantum information [17].

We now investigate the spectrum of down-converted photons under the influence of focused pumping as shown in Fig. 6. Here, we assume the coincidence collection scheme as in Fig. 1 for measuring the spectrum. Also, we used the Sellmeier equation of the BBO crystal for the simulation. The optic axis is assumed to be properly aligned to get collinear and non-collinear SPDC. Since we assumed that the pump beam is cw coherent light, the frequency of idler photon is uniquely determined by the signal photon: $\omega_i = \omega_p - \omega_s$. Also, if we assume a perfect monochromator, $\delta(\omega_s - \omega_m)$, in the signal arm for spectrum measurement, the two-photon amplitude becomes,

$$\begin{aligned}
|\mathcal{A}_{12}| \propto & \int d\omega_s \int d\omega_i\, \delta(\omega_s - \omega_m)\delta(\omega_p - \omega_s - \omega_i) \\
& \times \exp[-w_0^2(\Delta_x^2 + \Delta_y^2)/4]\,\mathrm{sinc}(L\Delta_z/2), \qquad (39)
\end{aligned}$$

where ω_m is the set frequency of the monochromator. The positions of the detectors are assumed to be fixed at $(\theta_x, \theta_y) = (0, 0)$ for the collinear case, and $(\theta_x, \theta_y) = (0, \pm 1.5\,^\circ), (0, \pm 3.0\,^\circ)$ for the non-collinear cases. The angular variables, ψ_s, ϕ_s, ψ_i, ϕ_i, are uniquely determined for each case. Therefore, the spectrum can be calculated to be,

$$S(\omega_s, w_0) \propto \left|\mathcal{A}_{12}\left(\omega_s, \omega_p - \omega_s, \vec{\theta_s}, \vec{\theta_i}, w_0\right)\right|^2. \tag{40}$$

Note that $\vec{\theta_s} = (\theta_{sx}, \theta_{sy})$ and $\vec{\theta_s} = (\theta_{ix}, \theta_{iy})$ are determined by the detector positions. From Eq. (40), we can simulate the spectral property of SPDC photons depending on the pump beam width (w_0). The full-width and half maximum (FWHM) is used as a measure of spectral width.

In Fig. 6, the horizontal axis is the pump beam width, so when the focusing becomes stronger, the beam width becomes smaller. The vertical axis is the full width at half maximum (FWHM) of the spectrum. Comparing Fig. 6(a) with (b), we can notice that the spectrum of the type-I SPDC is much broader than that of type-II SPDC. Also, the spectrum of type-I SPDC is relatively sensitive to the focusing condition than the spectrum of type-II SPDC.

For collinear SPDC, the spectrum is not affected by the pump focusing condition. This is because the photons propagating in collinear direction has $\psi_j = 0$ so that the phase mismatches in x and y direction will be identical to zero, i.e. $\Delta_{x,y} = 0$, see Eq. (22). The Gaussian function becomes unity, i.e. $\exp[-w_0^2(\Delta_x^2 + \Delta_y^2)/4] = 1$, and the spectrum is solely determined by the sinc function. For example, for type-I SPDC,

$$|\mathcal{A}_{12}| \propto \mathrm{sinc}\left[\frac{L}{2}\left(K_p(\omega_p, \Psi) - K_s'(\omega_s) - K_i'(\omega_i)\right)\right]. \tag{41}$$

Hence, the pump focusing cannot affect the two-photon amplitude for collinear case.

The spectrum for non-collinear SPDC shown in Fig. 6 is broadened as the pump is more focused. As seen in Eq. (26), the two-photon amplitude is determined by the Gaussian function and the sinc function. Let us take a look at the Gaussian function,

$$\exp[-w_0^2(\Delta_x^2 + \Delta_y^2)/4]. \tag{42}$$

When the pump beam width, w_0, is large the phase mismatches $\Delta_{x,y}$ should be close to 0 to have the significant probability of detection, so the Gaussian function more tightly limits the frequency spectrum. When the pump is more focused, i.e. when the pump beam width w_0 becomes small, more non-zero $\Delta_{x,y}$ are allowed so that the limitation of the spectrum by the Gaussian function is released accordingly. For type-I SPDC, when the pump beam width is very small, $w_0 \approx \propto 0$, the spectrum becomes as broad as the collinear case as shown in Fig. 6(a). This is because the Gaussian function becomes unity in the limit $w_0 \to 0$ and the sinc function becomes,

$$\mathrm{sinc}\left[\frac{L}{2}\left(K_p(\omega_p, \Psi) - K_s'(\omega_s) - K_i'(\omega_i)\right)\right]. \tag{43}$$

Note that the collinear case and the non-collinear case are identical for type-I SPDC, which is shown as the meeting line near $w_0 = 0$. However, unlike in type-I SPDC, in type-II SPDC, the spectrum of non-collinear SPDC does not become identical to that of collinear SPDC as $w_0 \to 0$. In Fig. 5(b), it is clearly observable that the lines (for collinear and for non-collinear SPDC) do not meet near $w_0 = 0$. This is because in type-II SPDC, the extraordinary signal photon has angular dependence in its refractive index, so the sinc function,

$$\mathrm{sinc}\left[\frac{L}{2}\left(K_p(\omega_p, \Psi) - K_s'(\omega_s, \Psi_s) - K_i'(\omega_i)\right)\right], \tag{44}$$

cannot be the same with the collinear case. Also, note that when the angle of detection in non-collinear SPDC is increased, the spectrum becomes narrower, as shown in Fig. 6. Note that the spectrum of SPDC in the positive uni-axial crystal (Urea), which is not shown in Fig. 6, has similar response to the pump focusing as the spectrum of the negative uni-axial crystal (BBO).

4. Conclusion

The spatial and spectral properties of entangled photons from SPDC with a focused pump are studied with theoretical analysis and numerical simulation, without invoking transverse momentum conservation assumption. Based on the two-photon amplitude expression calculated in Section 2, in which all properties of photon pairs are reflected, we have obtained the spatial and spectral properties of SPDC photons under focused pumping in various SPDC configurations, including type-I, type-II for both positive and negative uniaxial crystals. In particular, the transverse walk-off of pump and SPDC photons are both responsible in change of spatial profiles. Changes in the spectral properties in response to pump focusing are also studied. This paper is to our best knowledge the first study that describes the effect of pump focusing in such generalized SPDC configurations. Our result not only helps to understand the effect of pump focusing in SPDC better but also can find use in application of SPDC in realizing quantum information protocols.

Acknowledgements

This work was supported by Samsung Science & Technology Foundation under Project Number SSTF-BA1402-07.

References

[1] Y.H. Shih, C.O. Alley, New type of Einstein–Podolsky–Rosen–Bohm experiment using pairs of light quanta produced by optical parametric down conversion, Phys. Rev. Lett. 61 (26) (1988) 2921–2924.
[2] C.K. Law, I.A. Walmsley, J.H. Eberly, Continuous frequency entanglement: effective finite Hilbert space and entropy control, Phys. Rev. Lett. 84 (23) (2000) 5304–5307.
[3] A. Rossi, G. Vallone, A. Chiuri, F. De Martini, P. Mataloni, Multipath entanglement of two photons, Phys. Rev. Lett. 102 (15) (2009) 153902.
[4] J. Leach, B. Jack, J. Romero, A.K. Jha, A.M. Yao, S. Franke-Arnold, D.G. Ireland, R. W. Boyd, S.M. Barnett, M.J. Padgett, Quantum correlations in optical angle-orbital angular momentum variables, Science 329 (5992) (2010) 662–665.
[5] Y.-H. Kim, W.P. Grice, Measurement of the spectral properties of the two-photon state generated via type-II spontaneous parametric down-conversion, Opt. Lett. 30 (2005) 908–910.
[6] S.-Y. Baek, Y.-H. Kim, Spectral properties of entangled photon pairs generated via frequency-degenerate type-I spontaneous parametric down-conversion, Phys. Rev. A 77 (4) (2008) 043807.
[7] S.-Y. Baek, Y.-H. Kim, Spectral properties of entangled photons generated via type-I frequency-nondegenerate spontaneous parametric down-conversion, Phys. Rev. A 80 (3) (2009) 033814.
[8] T.P. Grayson, G.A. Barbosa, Spatial properties of spontaneous parametric down-conversion and their effect on induced coherence without induced emission, Phys. Rev. A 49 (4) (1994) 2948–2961.
[9] M.H. Rubin, Transverse correlation in optical spontaneous parametric down-conversion, Phys. Rev. A 54 (6) (1996) 5349–5360.
[10] C.I. Osorio, A. Valencia, J.P. Torres, Spatiotemporal correlations in entangled photons generated by spontaneous parametric down conversion, New J. Phys. 10 (11) (2008) 113012.
[11] P.J. Mosley, J.S. Lundeen, B.J. Smith, P. Wasylczyk, A.B. U'Ren, C. Silberhorn, I. A. Walmsley, Heralded generation of ultrafast single photons in pure quantum states, Phys. Rev. Lett. 100 (13) (2008) 133601.
[12] W.P. Grice, I.A. Walmsley, Spectral information and distinguishability in type-II down-conversion with a broadband pump, Phys. Rev. A 56 (2) (1997) 1627–1634.
[13] W.P. Grice, A.B. U'ren, I.A. Walmsley, Eliminating frequency and space-time correlations in multiphoton states, Phys. Rev. A 64 (6) (2001) 063815.
[14] Z. Zhao, K.A. Meyer, W.B. Whitten, R.W. Shaw, R.S. Bennink, W.P. Grice, Observation of spectral asymmetry in cw-pumped type-II spontaneous parametric down-conversion, Phys. Rev. A 77 (6) (2008) 063828.
[15] S. Carrasco, M.B. Nasr, A.V. Sergienko, B.E.A. Saleh, M.C. Teich, J.P. Torres, L. Torner, Broadband light generation by noncollinear parametric down-conversion, Opt. Lett. 31 (2) (2006) 253–255.
[16] S. Carrasco, J.P. Torres, L. Torner, A.V. Sergienko, B.E.A. Saleh, M.C. Teich, Spatial-to-spectral mapping in spontaneous parametric down-conversion, Phys. Rev. A 70 (4) (2004) 043817.
[17] R.S. Bennink, Y. Liu, D.D. Earl, W.P. Grice, Spatial distinguishability of photons produced by spontaneous parametric down-conversion with a focused pump, Phys. Rev. A 74 (2) (2006) 023802.

[18] P.S.K. Lee, M.P. Van Exter, J.P. Woerdman, How focused pumping affects type-II spontaneous parametric down-conversion, Phys. Rev. A 72 (3) (2005) 033803.
[19] H. Di Lorenzo Pires, F.M.G.J. Coppens, M.P. van Exter, Type-I spontaneous parametric down-conversion with a strongly focused pump, Phys. Rev. A 83 (3) (2011) 033837.
[20] C.H. Monken, P.H. SoutoRibeiro, S. Pádua, Optimizing the photon pair collection efficiency: a step toward a loophole-free Bell's inequalities experiment, Phys. Rev. A 57 (4) (1998) R2267.
[21] C. Kurtsiefer, M. Oberparleiter, H. Weinfurter, High-efficiency entangled photon pair collection in type-II parametric fluorescence, Phys. Rev. A 64 (2) (2001) 023802.
[22] F.A. Bovino, P. Varisco, A. Maria Colla, G. Castagnoli, G. Di Giuseppe, A. V. Sergienko, Effective fiber-coupling of entangled photons for quantum communication, Opt. Commun. 227 (4) (2003) 343–348.
[23] A.M. Pérez, F. Just, A. Cavanna, M.V. Chekhova, G. Leuchs, Compensation of anisotropy effects in a nonlinear crystal for squeezed vacuum generation, Laser Phys. Lett. 10 (12) (2013) 125201.
[24] A. Cavanna, A.M. Pérez, F. Just, M.V. Chekhova, G. Leuchs, Compensation of anisotropy effects in the generation of two-photon light, Opt. Express 22 (8) (2014) 9983–9992.
[25] M. Fedorov, M. Efremov, P. Volkov, E. Moreva, S. Straupe, S. Kulik, Anisotropically and high entanglement of biphoton states generated in spontaneous parametric down-conversion, Phys. Rev. Lett. 99 (6) (2007) 063901.
[26] M.V. Fedorov, M.A. Efremov, P.A. Volkov, E.V. Moreva, S.S. Straupe, S.P. Kulik, Spontaneous parametric down-conversion: anisotropical and anomalously strong narrowing of biphoton momentum correlation distributions, Phys. Rev. A 77 (2008) 032336.
[27] Y. Jeronimo-Moreno, R. Jáuregui, Type-I parametric down conversion of highly focused Gaussian beams in finite length crystals, J. Opt. 16 (6) (2014) 065201.
[28] M.H. Rubin, D.N. Klyshko, Y.H. Shih, A.V. Sergienko, Theory of two-photon entanglement in type-II optical parametric down-conversion, Phys. Rev. A 50 (6) (1994) 5122–5133.
[29] T.B. Pittman, D.V. Strekalov, D.N. Klyshko, M.H. Rubin, A.V. Sergienko, Y. H. Shih, Two-photon geometric optics, Phys. Rev. A 53 (4) (1996) 2804–2815.
[30] K. Kato, Second-harmonic generation to 2048 Å in β-BaB_2O_4, IEEE J. Quantum Electron. 22 (1986) 1013–1014.
[31] W.R. Donaldson, C. Tang, Urea optical parametric oscillator, Appl. Phys. Lett. 44 (1) (1984) 25–27.